COBEM 2021 26th International Congress of Mechanical Engineering
November 22-26, 2021, Virtual Congress, Brazil

COB-2021- 2052
OPTIMIZATION OF LASER MICROMILLING PROCESS PARAMETERS FOR TEXTURING OF NUCLEATION SITES

Gabriel Serafin Couto Vieira
Milton Pereira
Mechanical Engineering Department, Federal University of Santa Catarina, Florianopolis, Brazil
gabriel.serafin@labtucal.ufsc.br
milton.pereira@ufsc.br

Marcia Barbosa Henriques Mantelli
Mechanical Engineering Department, Federal University of Santa Catarina, Florianopolis, Brazil
marcia@labtucal.ufsc.br

Abstract. *Many technologies rely on the precise handling of small volumes of fluid to work, with even microscale geometric enhancements to surface capable of yielding significant results. Surface enhancements in phase change applications are examples of interaction between liquids and surfaces. As such, they can be heavily influenced by the presence or absence of appropriate-sized cavities. The use of enhanced surfaces in thermosyphons is accepted to speed up bubble nucleation. Depending on the inner conditions of thermosyphon, a delay in bubble nucleation may lead to unwanted energy accumulation and even occasional geysering of the working fluid (i.e., GBP, the Geyser Boiling Phenomenon). While laser texturing is applicable in solutions where precision is crucial, the risk of burr formation can be a deterrent. Although these burrs are also microscopic, they may negatively influence the bubble nucleation and active nucleation site viability. As such, laser texturing can become a much more viable option for heat transfer enhancement if these challenges are solved. This work aims to investigate which strategies are appropriated for nanosecond pulsed laser micromachining to create burr-free nucleation sites. First, the conditions inside a thermosyphon will be calculated on basis of experiments surrounding the investigation of the GBP. Afterward, the optimal nucleation sites for these conditions will also be calculated. Parameter combinations such as power, pulse length, and the number of pulses over the same area which lead to these optimized nucleation sites will be investigated. This work will also present options to either avoid burr formation. Lastly, a brief discussion on the viability and the possible applications will be presented.*

Keywords: *laser micromachining, burr free structures, optimized parameters, nucleation sites.*

1. INTRODUCTION

In many engineering applications, liquid vaporization occurs by transferring heat through the solid walls of some containing structure. In such cases, the hottest liquid in the system will be in the region immediately adjacent to the wall. If enough heat is added to the system, the liquid near the wall may even slightly exceed the equilibrium saturation temperature. Since the temperature is the highest at the solid-liquid interface, the formation of a vapor bubble embryo is likely to occur at this place. Eventually, this can take the form of distinct vapor bubbles, jets or films. According to Jabardo (2008), nucleated boiling is one of the most efficient mechanisms of heat transfer from a heated surface.

The importance of surface conditions on nucleated boiling has long been recognized. It is also known that there is an intricate relation between the cavity size and the surface-to-bulk temperature difference. Given the size scale in which these phenomena happen, it is expected that even microscopic details can influence bubble nucleation. As such, precise manufacturing solutions are recommended in applications that require the delicate handling of fluids and fluid-surface interaction.

The relation between the heat transfer rate (q'') and the excess temperature ($T_s - T_{sat}$) is depicted in Figure 1.

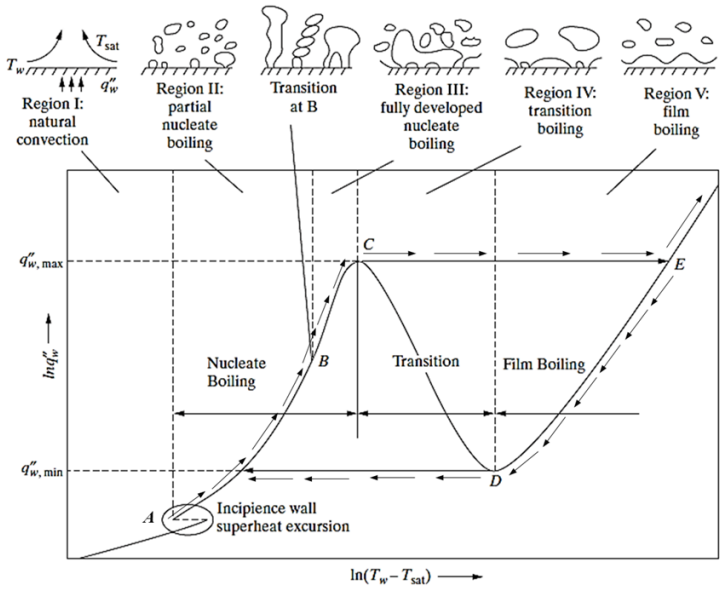

Figure 1 Nukiyama's curve - Nucleate boiling regimes. Source: Adapted from Guiaasiaan (2008).

In regards to the phenomena observed during boiling, the graph can be divided into five regions: natural convection (I), partial nucleate boiling (II), fully developed nucleate boiling (III), transition boiling (IV) and film boiling (V). Under this classification, natural convection (I) occurs at a very low excess temperature, without the presence of bubbles on the surface. With temperature increases, bubble nucleation will take place and can be divided into partial (II) and fully developed nucleated boiling (III). However, it should be noted that after a certain temperature excess, the bubbles formed on the surface coalesce, forming a vapor film (V). At this point, the contact between liquid and heated surface becomes obstructed by vapor, which leads to partial or complete drying of the surface (critical heat flux, $q''_{w,max}$, is reached). Since vapor impedes the liquid phase from actually reaching the surface, the heat exchange is affected and leads to an overheating of the surface.

According to Milanez and Mantelli (2005), thermosyphons are high-efficiency heat transfer devices: they can transfer heat at a very high rate with a relatively small temperature drop. They are enclosed, passive two-phase heat transfer devices, constituted by a closed, vertically oriented container, where a certain amount of working fluid is inserted. As stated by Faghri (1995), the high thermal conductance of the thermosyphons is directly associated with the high convection coefficients of the boiling and condensation observed internally in the device.

Under certain conditions, users of thermosyphon technology may be faced with the Geyser Boiling Phenomenon (GBP). This phenomenon occurs when the liquid pool is unable to sustain a constant ebullition, which leads to thermal energy accumulation on the system. When the conditions for bubble nucleation are finally met, what happens is a violent and intermittent bubble outburst. While the go-to solution to the problem is to increase the input heat flux, this is not always possible, especially if the device's heat transfer limit is reached before the conditions the GBP disappears.

In recent years, many works focus on ways of using surface texturing to increase the heat transfer coefficients (making the curve A-B-C steeper) and/or critical heat flux (increasing the value of $q''_{w,max}$). However, it should also be noted that if appropriate-sized nucleation sites are present, the temperature excess required to initiate nucleated boiling can be decreased (point A dislocated leftwards). As a practical consequence, the higher the number of nucleation sites, the lower the necessary temperature excess to initiate boiling and lower the level of accumulated energy. According to Guo *et al.* (2017), laser texturing is an interesting alternative to create a surface finish with relatively high machining accuracy while maintaining high processing speeds and low costs.

As such, this work aims to investigate which strategies are appropriated for laser micromachining to create nucleation sites. While the end goal of this investigation is to create appropriate-sized nucleation sites to decrease the energy storage level observed in the GBP, the first step of the investigation is to access the appropriated parameter combinations (*i.e.*, power, scanning velocity and the number of pulses over the same area). In future works, these nucleation sites can prevent energy accumulation inside thermosyphons and decrease the severity of the GBP.

2. LITERATURE REVIEW

2.1 Nucleation site geometry

Liquid boiling occurs when liquid comes into contact with a solid surface with a temperature sufficiently larger than the liquid saturation temperature. Griffith and Wallis (1958) stated that nucleation from a single cavity can be influenced

by the cavity geometry in two ways: firstly, the cavity diameter determines the superheat needed to initiate boiling, and secondly, its shape determines its stability once boiling begins.

Hsu (1962) proposed a set of equations to define the maximum and minimum sizes of effective cavities as functions of subcooling, thermophysical properties of the system and thickness of the superheated liquid layer. The waiting time was also used as criterion to differentiate effective and dead nucleation sites. Nucleation sites which present a finite waiting time (period between two bubble nucleation) and cavity size between the maximum and minimum limits are characterized as active nucleation sites. Furthermore, it is also noted that beyond appropriate size, cavities also "compete" with other cavities on its surroundings; if two cavities with proper conditions are nearby, the one with the shorter waiting time will always be preferred.

The mathematical model to estimate the size of the nucleation site was proposed by Hsu (1962) and ultimately proposes two equations to estimate the maximum and minimum (Equation 1) cavity radii:

$$r_c = \left(\frac{\delta}{2C_1}\right)\left[\left(1-\frac{\theta_{sat}}{\theta_w}\right) \pm \sqrt{\left(1-\frac{\theta_{sat}}{\theta_w}\right)^2 - \frac{4AC_3}{\delta\theta_w}}\right], \quad (1)$$

Where the meaning of the symbols is given in Table 1.

Table 1. Constants to Hsu's nucleation site model.

Symbol	Meaning	Unit
δ	Limiting thermal-layer thickness	$[m]$
C_1	Constant	-
C_3	Constant	-
θ_w	Temperature excess at the wall - $\theta_w = T_{wall} - T_{fluid}$	$[°C]$
T_{wall}	Wall temperature	$[°C]$
T_{fluid}	Working fluid temperature	$[°C]$
θ_{sat}	Temperature excess at saturation - $\theta_{sat} = T_{sat} - T_{fluid}$	$[°C]$
T_{sat}	Fluid saturation temperature	$[°C]$
A	Parameter representing $2\sigma T_{sat}/h_{lv}\rho_v$	$[m°C]$
σ	Surface tension of the liquid with respect to its vapor	$[N/m]$
h_{lv}	Latent heat of vaporization	$[J/kg]$
ρ_v	Vapor density	$[m^3/kg]$

*the author suggests values for δ, C_1 and C_3, respectively, as $7.62 * 10^{-5}[m]$, 2 and 1.6.

2.2 Geyser Boiling Phenomenon

The Geyser Boiling Phenomenon is a well-known problem to users of thermosyphon technology. One of the earliest references to geysering in two phase closed thermosyphons was done by Casarosa, Latrofa and Shelginski (1983), who studied the operation of closed two-phase thermosyphons, through a glass thermosyphon and observed an intermittent, pulsating boiling regime. This phenomenon was named "Geyser Effect". They found that the frequency of the Geyser effect increases with the heat flux in the evaporator, with its intensity dropping progressively until the effect disappears completely.

Kuncoro *et al.* (1995) presented an experimental study on the mechanism of geysering in a closed two-phase thermosyphon. The thermosyphon was made of glass and water and R113 were used as working fluids. It was found that as the wettability and surface tension of R113 present larger values than those of water, it influences on the device's performance, requiring more overheating before the nucleation. It was theorized that the accelerated expansion of the bubble is a dominant mechanism at the beginning of the Geyser Boiling, as a result of the thermal energy accumulation.

Pabón *et al.* (2019) presented an in-depth study of the Geyser Boiling phenomenon. A test bench consisting of a glass thermosyphon with a punctual heater enabled the study of the bubble dynamic during the occurrence of this phenomenon. A high-speed camera, a pressure transducer and thermocouples installed inside the thermosyphon allowed the characterization of the GBP. The analysis of the images and the pressure measurements suggested the existence of different levels of energy storage during the formation of bubbles. It was found that the pressure difference (ΔP) increment is proportional to the liquid column above the nucleation site. The closer the nucleation site is to the free liquid surface, the sooner the burst takes place and less energy is stored in the pool. Figure 11 depicts a series of images taken with a high speed camera on the precise moment of a bubble nucleation.

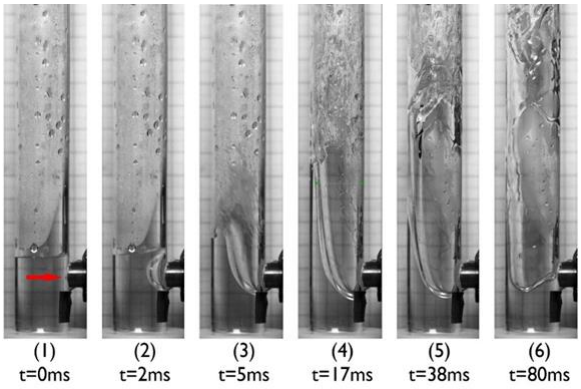

Figure 2 Experimental observation of the ebullition near the liquid free pool surface. (Source: Pabón *et al.* (2019)).

While the depicted phenomenon is divided in a number of steps, for the current analysis, only Figure 2.1 to Figure 2.3 are relevant. The arrow in Figure 2.1 indicates the exact point where the nucleation of the bubble was initially perceived. In the following images, Figure 2.1 to Figure 2.3, it is possible to observe the rapid growth of the bubble in a very short period. For this filling, the bubble takes only 5ms to reach the free surface of the pool and release its stored energy. At this point, it is observed that the bubble blasts and vapor and liquid are expelled towards the condenser, as a spray. Due to the smooth nature of the glass involucre, a considerable amount of thermal energy was stored, as evident by the violence in which the bubble burst.

2.3 Laser surface texturing

In laser machining, a beam irradiadiates a solid or liquid surface up to a point at which the material is removed from the bulk body (ablation of the material). According to Poprawe (2017), the ablation process can be divided in basically in two domains: Melt- and vapor-dominated ablation. The difference between these two forms of ablation is depicted in Figure 3.

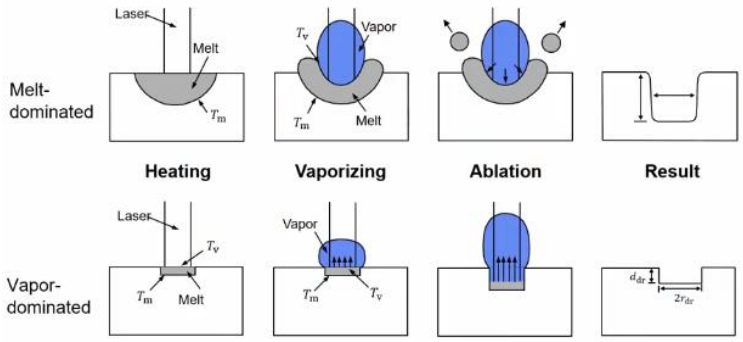

Figure 3 Melt-dominated and vapor-dominated ablation. (Source: Poprawe (2017)).

In the melt-dominated ablation, the laser beam irradiates the surface up to a point that a portion is melted to a melt pool. Then, the temperature increases in such way that vaporization is achieved, forming plasma. As a consequence, the vapor pressure pushes the melted material away from the laser-induced plasma vicinity. The final form of the obtained cavity will depend on the resolidification of the melted material.

On the other hand, if the intensity of the ablation process is increased, the vaporization will be the dominating material removal mean, and the process will present no significant melt pool portion. In this case, the removed material will be expelled in vapor state and the geometry of the cavity will be much more dependent on the shape of the laser beam.

Especially in the case of the melt-dominated domain, the energy of laser beam is absorbed when the material surface is irradiated by a laser pulse. The absorbed energy is subsequently converted into thermal energy, rapidly increasing the temperature of the beam irradiation spot. In turn, the material under the irradiation spot is then then melted and vaporized. Melt ejection is the governing mechanism of mass removal in this case; part of the molten liquid is immediately ejected into the air, while another part will instead flow along the cavity wall under the combined action of assist gas pressure and/or vaporization pressure. The latter is actually the material source of burr, as it flows toward the exit, then breaks up into discrete droplets due to surface tension effects when it reaches the exit rim.

According to Guo *et al.* (2017), laser texturing is an interesting alternative to create a surface finish with relatively high machining accuracy while maintaining high processing speeds and low costs. Martendal (2020) tested several laser machining parameters against electrolytic copper plates. The experiments were conducted with an IPG YLPN-1-1x120-50-M nanopulse fiber laser machine. As this work will be conducted with the same machine and workpiece material, the parameters described in the work will serve as a base for future experiments.

A sequence of individual laser pulses was emitted over a copper workpiece. Images were taken with a scanning electron microscope (SEM) and the obtained craters were measured with help of a MATLAB algorithm. Figure 4 shows the average crater diameters and respective standard deviation as a function of pulse power and pulse length.

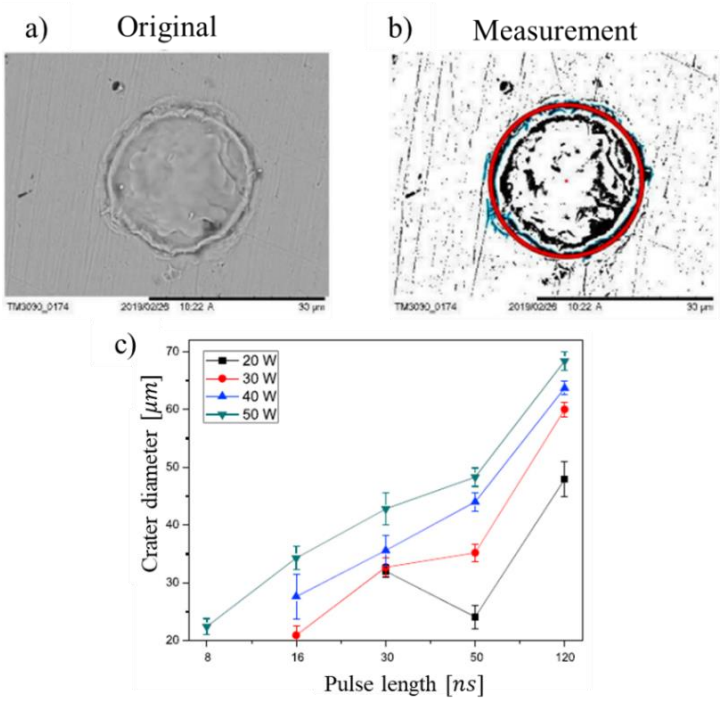

Figure 4. Resulting craters a)Crater MEV image; b) Crater diameter measurement with help of the MATLAB software algorithm and c) Crater diameter as a function of pulse power and pulse length.(Adapted from Martendal (2020))

As expected, the general trend for the crater diameter is that higher power levels yield larger craters. This trend mostly is followed for craters at 20 to $50W$. In a similar vein, the larger the pulse length, the wider the generated crater diameter. However, for experiments with the power setting of $20W$, craters were only considered to machined at pulse lengths of $30ns$ with the craters generated by pulse lengths of $50ns$ being actually smallest value. This indicates that the energy level in pulses under these configurations are not enough to incur in material removal from the bulk body.

Duan *et al.* (2015) experimentally studied the effect of machining parameters on the burr deposition in trepanning drilling. The experimental setup was a lamp pumped 300 W GSI JK300D Nd:YAG laser incorporated into a three-axis CNC machine, and a co-axial gas nozzle was used to provide nitrogen as assist gas. These single-factors experiments were designed to study the effect of: Pulse width; Pulse energy; Repetition rate; Trepanning diameter; Trepanning velocity; Beam rotation times; Assist gas pressure.

The factors were divided in two categories: those that affect the dynamic characteristics of this molten material (*D*) and those that affect the quantity of molten material (*Q*). The final effect of these analysis is summarized in Table 2.

Table 2 - Summary of process parameter effects on burr deposition.

Factor	Type of effect	Intensity of effect	Effect on burr formation
Pulse width	*Q/D*	Significant	- Increases with the increase of pulse width on early stages - Decreases with the further increment,
Pulse energy	*Q/D*	Significant	- Increases linearly with the increase of pulse energy
Pulse repetition rate	*Q/D*	Significant	- Increases with the increase of the repetition rate

Trepanning diameter	*Q*	Significant	- Increases directly with trepanning diameter.
Trepanning velocity	*Q*	Significant	- For low velocities, the pulse distribution density is too high, which leads to more molten material is generated, most of it is ejected; - For high velocities, the pulse distribution density is low, which leads to less molten material and thicker recast layer;
Beam rotation number		Little	- Burr volume is mainly determined by the first rotation.
Assist gas pressure	*Q/D*	Significant	- Initially, the gas flow interacts with the molten material, increasing its removal rate - If the outlet pressure is too great, the burr formation will grow again

As mentioned before, due to the delicate nature of bubble nucleation, the closer a crater is to an idealized nucleation site, the more accurate the models are. In this case, the sought after characteristic is a burr-free cavity. As such, as soon as the range of parameters for the experiment is chosen, the optimum combination would be expected as with pulse energy and repetition rate to be on the lower end of the spectrum, while pulse width is expected to be in the higher end.

Furthermore, it should be noticed that the laser texturing strategy of this work is different than the one utilized by Duan *et al.* (2015). As such, certain parameters in Table 2 do not pertain the present work, namely velocity, trepanning diameter and assist gas pressure.

3. EXPERIMENTAL PROCEDURE

3.1 Information workflow

As mentioned in the introduction, the project requirements are dependent on the experimental data of a thermosyphon operating with Geyser Boiling. As such, a number of data analysis and experimental processes will be carried out. The information workflow that will guide this work is depicted in Figure 5.

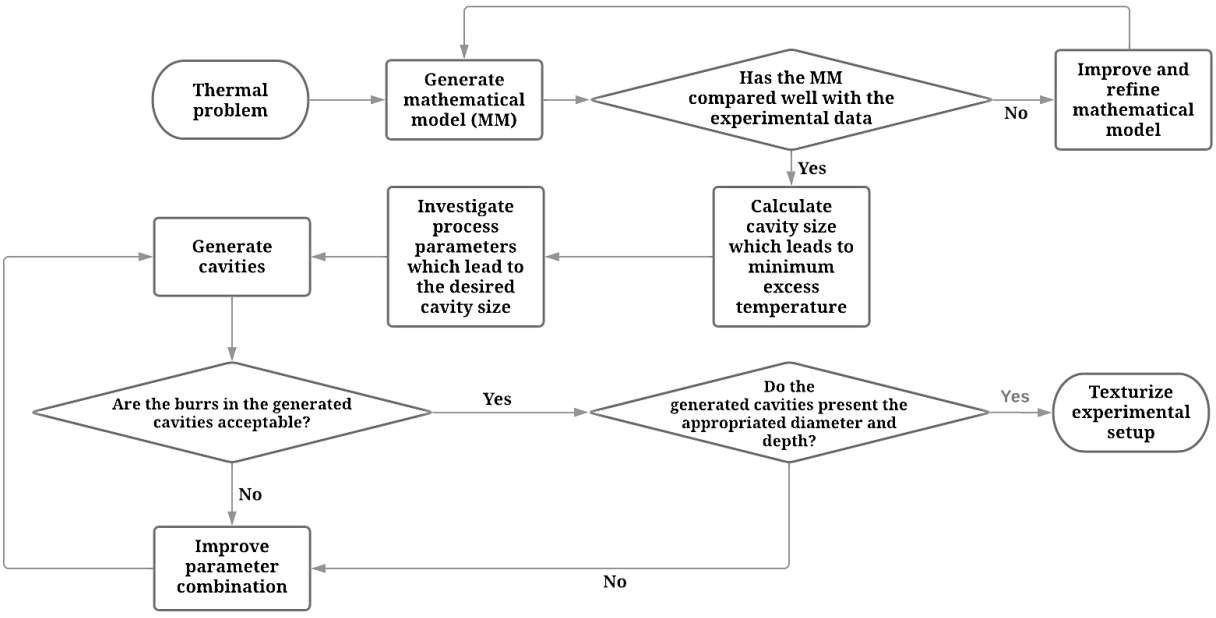

Figure 5. Expected tasks workflow

As seen in Figure 5, the analysis begins with the data from the thermal problem at hand. This dataset will then be used to create a mathematical model (MM) of the problem, as the measuring instruments cannot be directly measure the conditions at the bubble nucleation. If the MM is considered satisfactory, then the information generated by it will be used to calculate the cavity size which leads to the minimum excess temperature (see Equation 1). As seen in Figure 4, by using certain combinations of process parameters, it is possible to predict the generated cavity size. After they are generated, they must be analyzed on terms of generated burr and crater size. If the results are considered satisfactory, then the parameter combination is considered validated and can be employed in actual thermosyphons.

3.2 Thermal problem

Data from the test results obtained by Pabón *et al.* (2019) are used to estimate the operation conditions for this work. The used data is given in Table 3 and a sketch of the simplifications required for this first assumption is given in Figure 6.

Table 3 - Averaged temperature before geysering.

Thermocouple	Averaged Temperature [°C]
Evp1	145,4
Evp2	146,5
Evp3	148,3
Res	146,9
Evp_G	40,8
Cnd_G1	39,4
T_amb	23,3

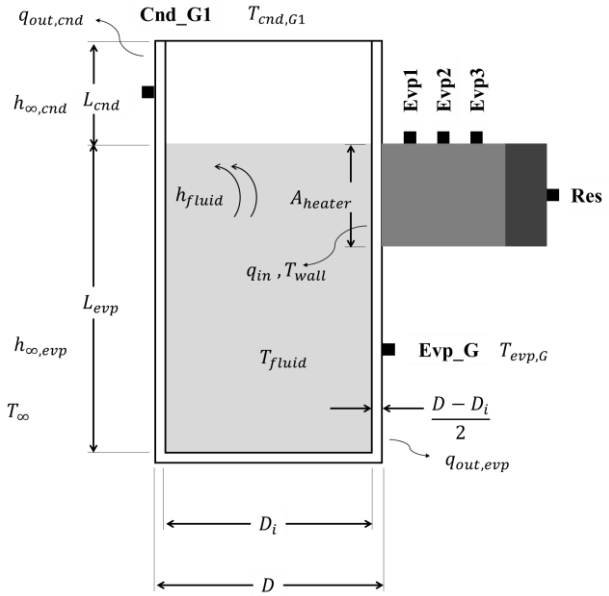

Figure 6. Simplification of the thermal problem.

The free convection heat transfer coefficients at the condenser ($h_{\infty,cnd}$) and evaporator pool ($h_{\infty,evp}$) sections are calculated as functions of the geometrical characteristics (*i.e.*, respective section lengths L and diameter D) and surface temperatures $T_{cnd,G1}$ and $T_{evp,G}$ and ambient air temperature T_∞. With $h_{\infty,cnd}$ and $h_{\infty,evp}$, it is possible to calculate the heat losses from the thermosyphon to the ambient air ($q_{out,cnd}$ and $q_{out,evp}$). Using $q_{out,evp}$ and considering the glass wall thermal resistance, it is possible to estimate the working fluid temperature, T_{fluid}.

In order to calculate h_{fluid}, a few hypotheses are assumed: free convection in the A_{heater} region; a non-dimensional model is used and the whole heat input influences directly on the liquid pool. As T_{wall} is not known, the problem is solved iteratively. These data and hypothesis were written in a EES code and the wall temperature is calculated as $132.5°C$.

After a comparison between this result and data from Table 3, it is reasonable to assume that the mathematical model is accurate. Under these hypotheses and varying the θ_w parameter in Equation 1, it is possible to calculate both the maximum and minimum expected nucleation site radii for the above conditions.

The results for $d_{c,max}$ and $d_{c,min}$ ($d_c = 2r_c$) were plotted and are depicted in Figure 7.

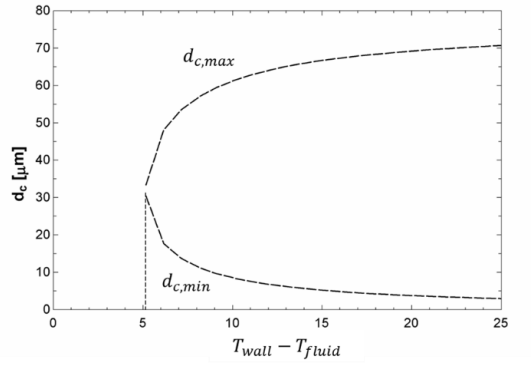

Figure 7. Diameter of active nucleation cavities as a function of temperature excess at the wall.

In Equation 1, the term θ_w is inside a root square, which justifies the shape of the curve depicted in Figure 7. Interestingly, after a degree of temperature excess at the wall, there is little influence over the size of the nucleation site. On the other hand, for a minimum temperature excess, the recommended nucleation site would be around 30μm.

3.3 Laser texturing

The quality of the surface texture will be closely monitored. Especial attention will be given to the burr formation on the heater surface. As described by Griffith and Wallis (1958), the cavity shape can affect the shape and diameter of a departing bubble while the cavity diameter affects the needed wall superheat. It is speculated that the burrs at the cavity rim can negatively interfere in bubble nucleation. They can influence on the contact angle of the vapor bubble and deviate the actual performance from the expected operation.

To machine viable nucleation sites, data presented by Martendal (2020) (see Figure 4), serves as a basis for the first Design of Experiments (DoE), which will aim to find the proper machining parameters. The DoE in question is presented in Table 4.

Table 4. Initial DoE for cavity manufacturing

N	***P***								
	30 *W*			**40 *W***			**50 *W***		
10	8 ns	16 ns	30 ns	8 ns	16 ns	30 ns	8 ns	16 ns	30 ns
20	8 ns	16 ns	30 ns	8 ns	16 ns	30 ns	8 ns	16 ns	30 ns

Where *P* is the pulse power and *N*, the number of pulses over the same area. The parameters above were chosen as a first hypothesis to reach the calculated range of values depicted in Figure 7.

4. RESULTS AND DISCUSSION

As seen from Table 4, the parameters are pulse power (P [W]), number of scanning passes (n) and pulse length (t [ns]). Power and pulse length possess three possibilities each and number of pulses, two. An association of these parameters yields 18 possible parameter combinations. Figure 8 depicts some of the obtained results and Table 5, their respective process parameters.

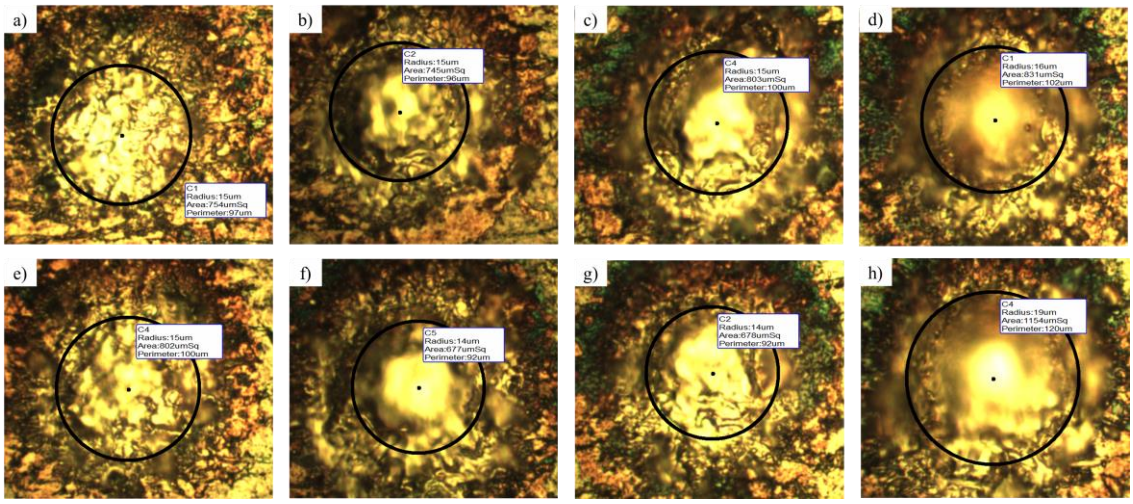

Figure 8 - Preliminary laser texturing results.

Table 5 - Process parameters and respective crater diameters

	n = 10		n = 20	
	16 ns	30 ns	16 ns	30 ns
$P = 30W$	$d_a = 30\mu m$	$d_b = 30\mu m$	$d_c = 30\mu m$	$d_d = 32\mu m$
$P = 40W$	$d_e = 30\mu m$	$d_f = 28\mu m$	$d_g = 28\mu m$	$d_h = 38\mu m$

As expected, the diameter of the proposed DoE was well within the expected values ($28 \leq d \leq 38\mu m$). As seen by the focus on Figure 8.a and Figure 8.c, the combination of pulse length $16ns$ and $n = 10$ is not enough to cause material removal. However, by increasing the pulse length from 16 to 30 ns (*i.e.*, increase of 90%) or the number of pulses from 10 to 20, the mark generated on the surface actually starts to resemble a crater. Apparently, for larger pulse lengths, the material removal is much more severe, with the disadvantage of burr formation at the crater's rim.

By comparing the results from Figure 8.d to Figure 8.h, by increasing the pulse power from 30 to 40 W (*i.e.*, increase in 33%), the resulting crater diameter actually increased. Again, this result was also expected, as seen in Figure 4.

Due to the lack of reliable measurements of both burr formation and crater depth, it is not possible to evaluate which parameter combination yielded the best results. On the other hand, it was observed during the visualization that the texturing presented features both over and under the microscope focus. These are believed to be, respectively, burrs and craters.

5. CONCLUSIONS

It is observed that the mathematical modeling was able to predict the wall temperature of the thermosyphon relatively well, as seen from a comparison between the wall temperature reached through the mathematical model and the experimental data.

In laser machining, the material removal process can be divided into two domains: Melt- and vapor-dominated ablation. In the melt-dominated domain, the final form of the obtained cavity will depend on the resolidification of the melted material. The burr formation in laser appears as the melted material flows toward the cavity exit, then breaks up into discrete droplets due to surface tension effects when it reaches the exit rim.

While the used DoE shows promising results regarding the diameter of the machined craters, it is difficult to ascertain the level of burr formation and crater depth. One way to solve this problem is to employ a new laser milling strategy: milling of a continuous trench, instead of craters. In this case, a sample could be mounted with a resin and prepared similarly to a metallographic analysis.

Only after the laser texturing wields favorable results (*i.e.*, with craters in the expected size range and free of burrs) it can be used on actual heat transfer applications. To study the effect of these nucleation sites, they must be machined onto a surface completely free of other potential nucleation sites. One possibility is to employ a punctual heater, similarly to Pabón *et al.* (2019). The area of interest must be polished and distant from any surface intersections, as far from potential nucleation sites as possible. Furthermore, the area must be monitored with thermocouples on the heat input area, its vicinity, and the bulk fluid itself.

6. REFERENCES

Casarosa, C., Latrofa, E., & A, S. 1983. The Geyser Effect in a two-phase Thermosyphon. *International Journal of Heat and Mass Transfer*, 26, pp. 933-941.

Duan, W., Wang, K., Dong, X., Xuesong, M., Wang, W., & Fan, Z. 2015. Experimental characterizations of burr deposition in Nd:YAG laser drilling: a parametric study. *International Journal of Advanced Manufacturing Technology*, 1529-1542.

Faghri, Amir. 1995. *Heat Pipe Science and Technology*. s.l. : Taylor & Francis Inc, 1995.

Griffith, P., & Wallis, J. D., 1958. "Technical Report No. 14 - The role of surface conditions in nucleate boiling." Cambridge 39, Massachusetts: Massachusetts Institute of Technology

Guiaasiaan, S. Mostafa. 2008. *Two-Phase Flow, Boiling and Condensation in conventional and Miniature Systems*. Cambridge : Cambridge University Press, 2008. Vol. 1.

Guo, J., Li, Y., Lu, H., Qin, L., Li, Y., & Dong, G. ,2017. "An effective method of edge deburring for laser surface texturing of Co-Cr-Mo alloy". *International Journal of Advanced Manufacturing Technology*, 1491-1503.

Hsu, Y., 1962. "On the Size Range of Active Nucleation Cavities on a Heating Surface". *Journal of Heat Transfer*, 207-213.

Incropera, F., de Witt, D., Bergman, T. L., & Lavinne, A. S., 2011. *Fundamentals of Heat and Mass Transfer*. Jefferson City: John Wiley & Sons.

Jabardo, J. 2008. Transferência de calor por ebulição e trocadores de calor bifásicos. Florianópolis: *1° Encontro Brasileiro sobre Ebulição, Condensação e Escoamento Múltifásico Líquido-Gás*.

Kuncoro, H., Rao, Y F and Fukuda, K. 1995. An Experimental study on the mechanism of geysering in a closed two-phase thermosyphon. *International Journal of Multiphase*. 6, 1995, Vol. 21, pp. 1243-1252.

Milanez, F. H., & (2005, September 15). Thermal characteristics of a thermosyphon heated enclosure. *International Journal of Thermal Sciences*, 45, 504 - 510.

Pabón, N. L., Mera, J. F., Vieira, G. S., & Mantelli, M. H., 2019. "Visualization and Experimental Analysis of Geyser Boiling Phenomena in Two-Phase Thermosyphons". *International Journal of Heat and Mass Transfer*.

Pereira Martendal, C., 2020. Texturização a Laser de Superfícies de Cobre para Aplicação em Transferência de Calor com Mudança de Fase. Dissertação de Mestrado, 102. Florianópolis, Santa Catarina, Brasil: Universidade Federal de Santa Catarina.

Poprawe, R. (2017, 12 21). Laser ablation and drilling. Aachen, North Rhine-Westphalia, Germany. Retrieved 11 13, 2019, from https://www.youtube.com/watch?v=ZHnm7t1NZPg

Smith, K., Kempers, R., & Robinson, A. 2018. Confinement and vapour production rate influences in closed two-phase reflux thermosyphons Part A: Flow regimes. *International Journal of Heat and Mass Transfer*, 19.

7. RESPONSIBILITY NOTICE

The authors are the only ones responsible for the printed material included in this paper.